Published on 22 October 2014. Downloaded by Trinity Western University on 16/01/2015 01:51:28.

RSC Advances

PAPER

View Article Online
View Journal | View Issue

Cite this: *RSC Adv.*, 2014, **4**, 56933

Giant piezoelectric properties of BZT–0.5BCT thin films induced by nanodomain structure

W. L. Li,*[ab] T. D. Zhang,[a] Y. F. Hou,[a] Y. Zhao,[a] D. Xu,[a] W. P. Cao[a] and W. D. Fei[ac]

Received 7th August 2014
Accepted 21st October 2014

DOI: 10.1039/c4ra08280j

www.rsc.org/advances

$Ba(Zr_{0.2}Ti_{0.8})O_3$–0.5$(Ba_{0.7}Ca_{0.3})TiO_3$ (BZT–0.5BCT) thin films were prepared from two ceramics targets, $Ba(Zr_{0.2}Ti_{0.8})O_3$ and $(Ba_{0.7}Ca_{0.3})TiO_3$, using dual-magnetron sputtering, and a $LaNiO_3$ (LNO) seed layer was introduced between the film and Pt(111)/Ti/SiO_2/Si substrates *via* a sol–gel technique. Domain structures were observed on the thin films by piezoelectric force microscopy (PFM), and then an autocorrelation function technique was applied to analyze the obtained PFM images. The mean sizes of the domains of the BZT–0.5BCT and (001)-oriented BZT–0.5BCT/LNO thin films are 69.2 nm and 151 nm at room temperature respectively. On the basis of our results, it is proven that the nanodomains have a large effect on the piezoelectricity of the thin films for MPB composition: the converse piezoelectric coefficient d_{33} is 258 pm V^{-1} for BZT–0.5BCT thin films and 122 pm V^{-1} for BZT–0.5BCT/LNO thin films. It is worth noting that not only the crystal orientation, but also the domain structures play critical roles in the piezoelectricity for the BZT–0.5BCT thin films. Furthermore, (001)-oriented BZT–0.5BCT/LNO thin films exhibit excellent dielectric properties and the dielectric constant ($\varepsilon \sim 1046$) is dramatically increased compared with the BZT–0.5BCT thin films ($\varepsilon \sim 168$). The *C*–*V* results indicate that both of the thin films are ferroelectric in nature.

Introduction

Lead-based compounds (PZT, PMN–PT),[1,2] which have been extensively applied in sensors, actuators, and energy harvesters,[3] are the most popularly used piezoelectric materials, due to their excellent piezoelectric properties. However, their wide application has caused many environmental problems because of the high toxicity of the high lead content in these piezoelectric materials. Therefore, many efforts have been made to search for lead-free candidates to replace lead-based ceramics and thin films. Recently, it was reported that 0.5$Ba(Zr_{0.2}Ti_{0.8})O_3$–0.5$(Ba_{0.7}Ca_{0.3})TiO_3$ (abbreviated as BZT–0.5BCT) ceramic shows a surprisingly high piezoelectric coefficient of $d_{33} \approx 620$ pC N^{-1} at the morphotropic phase boundary (MPB),[4] and is considered to be one of the most important lead-free substitutes that can be comparable to PZT.

BZT–*x*BCT thin films offer several advantages over their bulk counterparts, such as lower driving voltages and the potential for integrated circuit with Si, and have attracted much attention from the research community. Although results from both G. Q. Kang *et al.*[5] and A. Piorra *et al.*[6] indicate that d_{33} of BZT–*x*BCT is less than 80 pm V^{-1}, which is smaller than that of PZT thin films (100–120 pm V^{-1} (ref. 7)), it is widely believed that excellent piezoelectricity would be obtained at the MPB where no or a lower energy barrier exists for the polarization rotation from the (001)T to the (111)R state.[8] Besides the MPB, the crystal orientation and the domain structure of thin films are also important factors for piezoelectricity.[9–12] It is well known that oriented BZT–*x*BCT piezoelectric thin films always show enhanced dielectric, ferroelectric and piezoelectric properties.[9,13,14] Furthermore, domain structure, especially with respect to configuration, plays a major role in ferroelectric switching in ferroelectric and relaxor-ferroelectric materials.[15] However, up to now there has been little research on studying how the domain structure and the crystal orientation affect the piezoresponse of BZT–0.5BCT thin films.[14] Piezoelectric force microscopy (PFM) has been successfully developed and subsequently used for the local characterization of piezoelectric materials at the nanometer scale, especially for static and dynamic polarization behaviors in ferroelectrics. PFM can describe polar nanosized regions (PNRs) or polar nanodomains (PNDs).[15,16]

In this study, the BZT–0.5BCT thin films were prepared by radio frequency dual-magnetron sputtering. With the help of PFM and autocorrelation techniques, the domain structure, piezoresponse, converse piezoelectric coefficients d_{33} and dielectric properties of the BZT–0.5BCT thin films with and without (001) preferred orientation are discussed and analyzed.

[a]School of Materials Science and Engineering, Harbin Institute of Technology, Harbin 150001, P. R. China. E-mail: wlli@hit.edu.cn; Fax: +86-451-86415894; Tel: +86-451-86415894

[b]National Key Laboratory of Science and Technology on Precision Heat Processing of Metals, Harbin Institute of Technology, Harbin 150001, P. R. China

[c]State Key Laboratory of Advanced Welding and Joining, Harbin Institute of Technology, Harbin 150001, P. R. China

www.spm.com.cn

Published on 22 October 2014. Downloaded by Trinity Western University on 16/01/2015 01:51:28.

Experimental

The $Ba(Zr_{0.2}Ti_{0.8})O_3$–$0.5(Ba_{0.7}Ca_{0.3})TiO_3$ thin films were prepared from two ceramics targets ($Ba(Zr_{0.2}Ti_{0.8})O_3$ and $(Ba_{0.7}Ca_{0.3})TiO_3$) using dual-magnetron sputtering. Prior to deposition, the targets were pre-sputtered for 10 min to eliminate surface heterogeneity, and then sputtered under an RF power of 40 W at 500 °C under an Ar and O_2 atmosphere with a pressure of 1.4 Pa.

A $LaNiO_3$ (LNO) seed layer was grown on Pt(111)/Ti/SiO_2/Si substrates using a sol–gel process. The first processing step was to spin-coat a thin LNO layer onto the Pt/Ti/SiO_2/Si substrate, followed by pyrolysis at 375 °C for 3 min, and then the seed layer was annealed at 750 °C for 30 min. Next, BZT–0.5BCT thin films were sputtered by off-axis RF magnetron sputtering on LNO/Pt(111)/Ti/SiO_2/Si. Finally, the resulting films were heated at 750 °C for 30 min for crystallization. Before performance testing, platinum electrodes as the top electrode with a size of 3.14×10^{-4} cm^2 were deposited by DC magnetron sputtering.

The crystalline structures of the thin films were analyzed by a Philips X'pert X-ray diffractometer (XRD) with Cu Kα radiation generated at 40 kV and 40 mA. We propose a universal fiber texture on the basis of ω-scan XRD. The cross-section micrograph of the thin film was obtained by SEM (Helios Nanolab600i) and the surface morphology of the thin films was observed by atomic force microscopy (CSPM5600 of Benyuan). The piezoelectric properties of the thin films, including PFM images and piezoelectric constants, were characterized by a commercial scanning force microscope (CSPM5600 of Benyuan) equipped with a lock-in amplifier (model SR530, Stanford Research Systems, Inc.). The PFM image measurements were performed in a piezoelectric contact mode, which is currently widely applied for the nanoscale characterization of domain structures. For domain visualization, ac voltage, with an amplitude of 1 V and a frequency of 20 kHz, was applied between the grounded tip and the bottom electrode. The piezoelectric constants of the samples were measured after poling ahead of time. In the poling process, the BZT–0.5BCT thin films were applied a voltage of 500 kV cm^{-1} for 10 min. For measurement of converse piezoelectric coefficients d_{33} in all films, the top platinum electrodes with the same size of 3.14×10^{-4} cm^2 were in contact with the conductive tip. The input ac sine wave voltage, with amplitude in the range of 0.5 V–3 V and a frequency of 5 kHz, which was chosen far away from the resonant frequencies of the cantilever acquiring the piezoelectric response during each pulse, was applied between the conductive tip and the bottom electrode in the thickness direction. The corresponding vertical deflection signal of the cantilever is recorded by a lock-in amplifier. By multiplying the deflection signal with the calibration constant of the photodetector sensitivity, the amplitude of the tip vibration was derived. The frequency dependence of the dielectric permittivity and the capacitance–voltage of the samples were measured using an Agilent 4294A precision impedance analyzer. The dielectric property measurements were performed at frequencies ranging from 10 kHz to 1 MHz. The capacitance–voltage property was measured with applied dc bias voltage from −10 V to 10 V.

Results and discussion

The XRD patterns of BZT–0.5BCT and BZT–0.5BCT/LNO thin films show pure perovskite-type structures with no detectable impurities or secondary phases. As shown in the inset of Fig. 1, a FWHM value of $\omega = 8.1°$ measured at the (100) peak indicates (001)-orientated growth attributed to the lattice mismatch and the interfacial effect between the LNO seed layer and the BZT–BCT thin films.

Both BZT–0.5BCT and BZT–0.5BCT/LNO films exhibit a uniform and dense surface structure as can be seen in Fig. 2. The grain size is 150 nm for the BZT–0.5BCT thin films and 177 nm for the BZT–0.5BCT/LNO thin films. In addition, the LNO seed layer has an obvious influence on the surface roughness of the thin films, *viz.*, 5.2 nm for the film with a LNO seed layer, which is smaller than the one without a LNO seed layer (9.8 nm). The SEM micrographs of the cross-sections of the films are given in Fig. 2(c) and (d). The scanning results show that the thickness of the films is approximately 200 nm and that the films have a dense microstructure at the microscopic scale.

Fig. 3 shows the representative PFM images measured on BZT–0.5BCT and BZT–0.5BCT/LNO thin films at room temperature. As shown in Fig. 3(a), the BZT–0.5BCT thin film consists of nanodomain regions with up and down polarizations and a mesh-like structure with slim and bright boundaries. Overall, the uniform distribution of the pattern of the mesh-like structure PNRs indicates good short-range ferroelectric order. For the sake of avoiding the effect of external signals, we chose the regions highlighted by the black frames with sizes of 1500 nm × 1500 nm for autocorrelation, where the influence of scanning lines can be avoided. In Fig. 3(b), the PFM image of the BZT–0.5BCT/LNO thin films has clearly visible grain boundaries

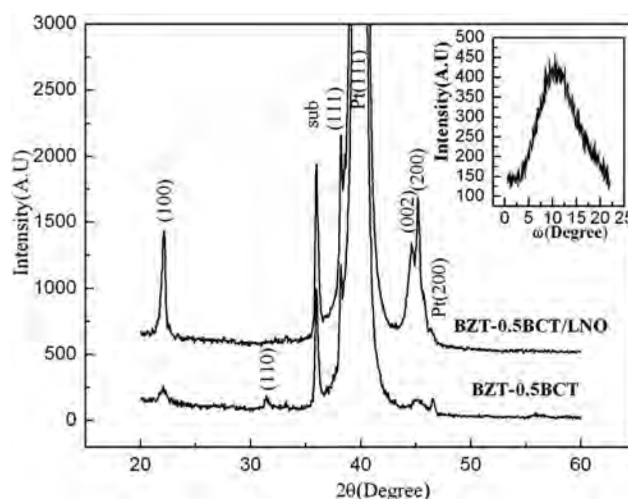

Fig. 1 XRD patterns of BZT−0.5BCT thin films without a LNO seed layer and BZT−0.5BCT thin films with a LNO seed layer; inset shows the XRD ω-scan for the (001)-oriented BZT−0.5BCT thin films with a LNO seed layer.

www.spm.com.cn

This journal is © The Royal Society of Chemistry 2014

Published on 22 October 2014. Downloaded by Trinity Western University on 16/01/2015 01:51:28.

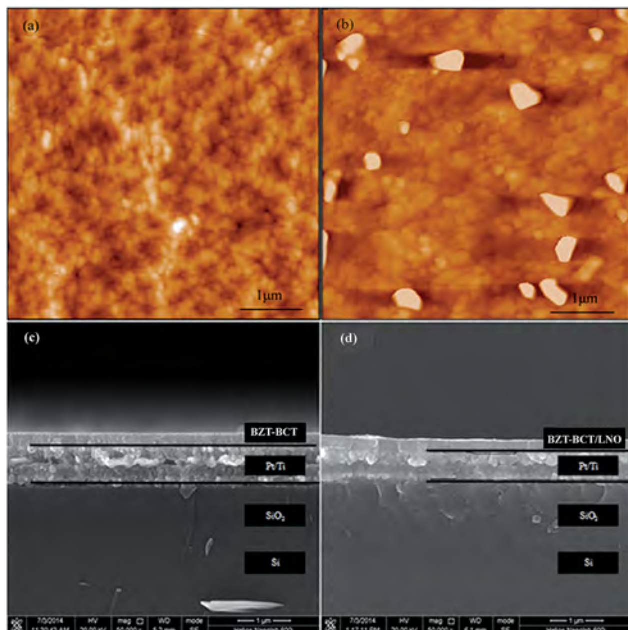

Fig. 2 AFM images of BZT–0.5BCT thin films (a) without a LNO seed layer and (b) with a LNO seed layer; SEM images of BZT–0.5BCT thin films (c) without a LNO seed layer and (d) with a LNO seed layer.

and a clear contrast between opposite polarities is observed. The size of these piezoactive regions varies in the range of hundreds of nanometers to micrometers. Their distributions show disorder on a large scale and the higher limit of the distribution may originate from the introduction of the LNO seed layer, so we chose the microdomain regions for analysis as reported by V. V. Shvartsman.[17] The 3D autocorrelation images of the BZT–0.5BCT and BZT–0.5BCT/LNO thin films, as shown in Fig. 3(c) and (d), were obtained from the original PFM *via* an autocorrelation transformation:

$$C(r_1, r_2) = \sum_{x,y} D(x, y) D(x + r_1, y + r_2)$$

where $D(x, y)$ is the value of the piezoresponse signal.

Autocorrelation analysis of the PFM data provided quantitative insight into the polarization distribution and nanodomain structure. Autocorrelation analysis was applied to estimate the size of the PNRs.[18–20] The autocorrelation function can be represented as a sum of two contributions:

$$C_{(r)} = A \exp\left[-\left(\frac{r}{\xi}\right)^{2h}\right] + (1 - A)\exp\left[-\frac{r}{r_c}\right]\cos\left(\frac{\pi r}{a}\right)$$

The first and second terms correspond to short range correlation and long range correlation, respectively. Only a short range correlation length term was taken into account for

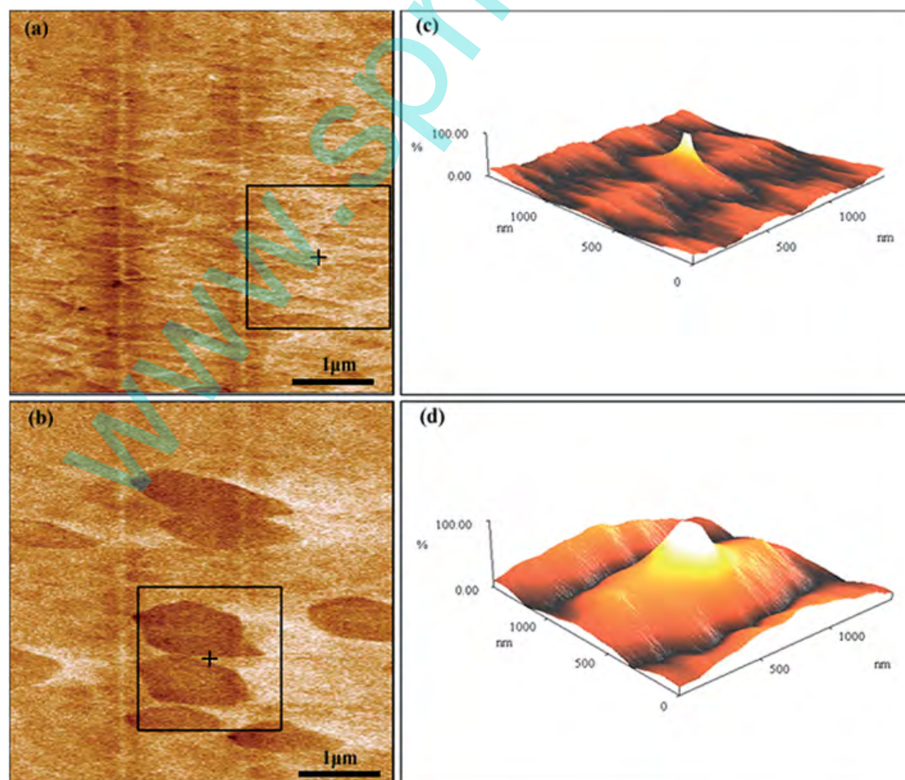

Fig. 3 PFM and autocorrelation images of BZT–0.5BCT thin films (a) PFM image of the thin film without a LNO seed layer and (b) PFM image of the thin film with a LNO seed layer; (c) autocorrelation image of the thin film without a LNO seed layer and (d) autocorrelation image of the thin film with a LNO seed layer.

www.spm.com.cn

Published on 22 October 2014. Downloaded by Trinity Western University on 16/01/2015 01:51:28.

thin films with uniform morphology[20], which was useful for the estimation of the characteristic parameters of the nanodomains. In this case, the experimental curves obtained from the cross sections of two-dimension autocorrelation images, as shown in Fig. 4, were approximately fitted with the first term:

$$C_{(r)} = A \exp\left[-\left(\frac{r}{\xi}\right)^{2h}\right]$$

here r is the distance from the central maximum, ξ represents the short range correlation length, and h ($0 < h < 1$) is a parameter related to the fractal dimension of the "polarization interface". A is the normalization constant.

Fig. 4(a) and (b) show the $C_{(r)}$ at a small r averaged over all in-plane directions. The short correlation length ξ, which is estimated from the best fit to $C_{(r)}$, is 69.2 nm for the BZT–0.5BCT thin films and 151 nm for the BZT–0.5BCT/LNO thin films, respectively. This indicates that the mean size of the nanodomains of the BZT–0.5BCT/LNO thin films is more than twice as large as that of the BZT–0.5BCT thin films. The larger size of the PNRs is due to stronger polar correlations in the thin films with a LNO seed layer. Furthermore, the interface induced by the LNO seed layer is more conducive to nucleation and aggregation for large nanodomains.

As shown in Fig. 5, both BZT–0.5BCT and BZT–0.5BCT/LNO thin films exhibit excellent piezoelectricity at room temperature, and the converse piezoelectric coefficients d_{33} are 258 pm V^{-1} and 122 pm V^{-1}, respectively, higher than 71.7 pm V^{-1},[5] 80 pm V^{-1},[6] and 100 pm V^{-1}.[9] The composition of the BZT–0.5BCT thin film is located at the MPB which has a low potential barrier for polarization rotation from the (001)T state to the (111)R state at room temperature,[8] giving rise to the outstanding piezoelectricity. Meanwhile, the encouraging results of the BZT–0.5BCT thin films without a LNO seed layer may be attributed to smaller nanodomain structures, domain states[21] and the existence of non-180° domains[9] in the random oriented-BZT–0.5BCT thin films which more easily enable polarization rotation compared to the larger nanodomains of the (001)-oriented BZT–0.5BCT/LNO thin films under the same external stimulation. The insertion of a LNO seed layer may provide nucleation sites and reduce the activation energy for the BZT–0.5BCT thin films, resulting in the better crystallization and the enhancement of the piezoelectric constant.

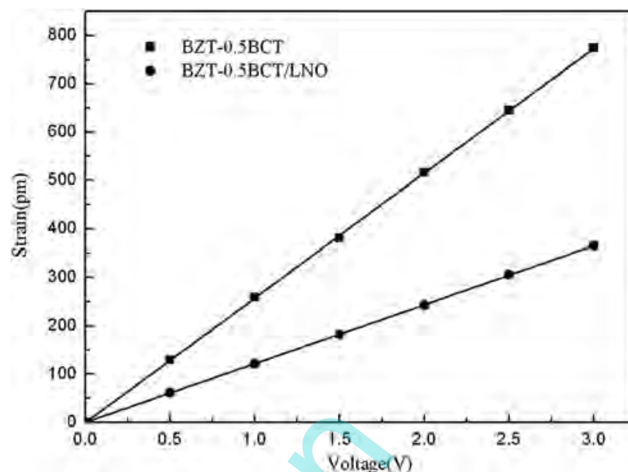

Fig. 5 Linear fit of experimental data for the converse piezoelectric coefficients d_{33} of the BZT–0.5BCT thin films (a) without a LNO seed layer and (b) with a LNO seed layer.

The dielectric properties of the BZT–0.5BCT thin films were measured at room temperature as a function of frequency ranging from 10 kHz to 1 MHz and are given in Fig. 6(a) and (b). The BZT–0.5BCT and BZT–0.5BCT/LNO thin films show their largest dielectric permittivities of 168 and 1064 at the frequency of 1 MHz. The dielectric losses of the films at 1 MHz are as low as 0.076 and 0.37. Fig. 6(c) and (d) show the capacitance–voltage (C–V) characteristics of the BZT–0.5BCT and BZT–0.5BCT/LNO thin films at room temperature and at the frequency of 1 MHz. The maximum capacitance values of the BZT–0.5BCT and BZT–0.5BCT/LNO thin films are 233 pF and 869 pF. The (001)-oriented BZT–0.5BCT/LNO film can manifest more excellent dielectric properties compared with the BZT–0.5BCT thin film, because the spontaneous polarization vector points are normal

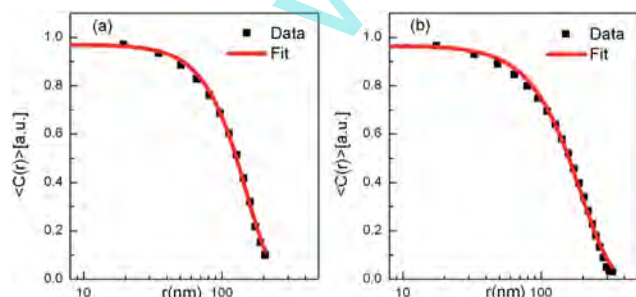

Fig. 4 Distance (r) dependence of the auto-correlation function ($C_{(r)}$), averaged over all in-plane directions. (a) corresponds to the 3D autocorrelation image in Fig. 3(c) and (b) corresponds to the 3D autocorrelation image in Fig. 3(d).

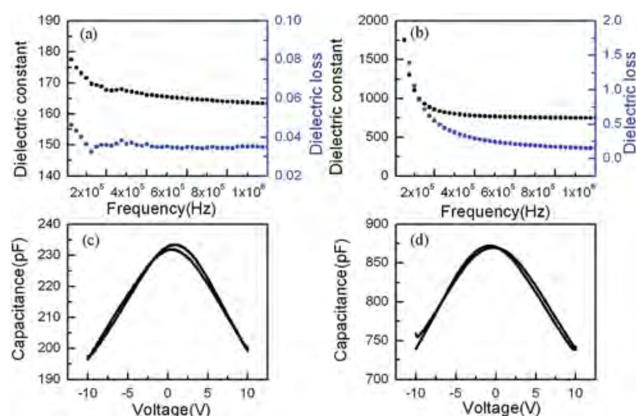

Fig. 6 Frequency dependence of dielectric permittivity and dielectric loss for BZT–0.5BCT thin films (a) without a LNO seed layer and (b) with a LNO seed layer; C–V curves of BZT–0.5BCT thin films at the frequency of 1 MHz (c) without a LNO seed layer and (d) with a LNO seed layer.

This journal is © The Royal Society of Chemistry 2014

Published on 22 October 2014. Downloaded by Trinity Western University on 16/01/2015 01:51:28.

to the (001)-oriented film surface and coincide with the dielectric measuring direction. The films' butterfly-shaped (*C*–*V*) curves which are caused by switching of the ferroelectric domains indicate that the films are ferroelectric in nature.[22] The curves are slightly asymmetrical on either side of the two branches, which may be attributed to the asymmetrical distribution of the space charge, oxygen vacancies[13] and the introduction of the LNO seed layer.

Conclusion

In summary, BZT–0.5BCT and BZT–0.5BCT/LNO thin films were prepared from two ceramics targets $Ba(Zr_{0.2}Ti_{0.8})O_3$ and $(Ba_{0.7}Ca_{0.3})TiO_3$ using dual-magnetron sputtering. The better crystallization and orientation of the BZT–0.5BCT/LNO thin film, which is caused by the insertion of a LNO seed layer, led to the relatively higher piezoelectric coefficient (122 pm V^{-1}). The large converse piezoelectric coefficient of ~258 pm V^{-1} is attributed to the smaller nanodomain size of ~69.2 nm in the BZT–0.5BCT thin films. By comparing the piezoelectricities of BZT–0.5BCT and BZT–0.5BCT/LNO thin films, it can been seen that the nanodomain structure rather than the crystal orientation has a more significant effect on the converse piezoelectric coefficient. Meanwhile, the crystal orientation is also conducive to the dielectric properties of BZT–0.5BCT thin films for MPB composition. With their excellent piezoelectric properties, the non-Pb BZT–BCT films are potential candidates for lead-free piezoelectric applications.

Acknowledgements

The authors gratefully acknowledge support from the Natural Science Foundation of China (Grant nos. 11272102 and 51202049).

References

1 G.-T. Park, J.-J. Choi, J. Ryu, H. G. Fan and H.-E. Kim, *Appl. Phys. Lett.*, 2002, **80**, 4606.
2 V. V. Shvartsman, A. L. Kholkin, I. P. Raevski, S. I. Raevskaya, F. I. Savenko and A. S. Emelyanov, *Appl. Phys. Lett.*, 2003, **113**, 187208.
3 E. Aksel and J. L. Jones, *Sensors*, 2004, **10**, 1935–1954.
4 H. X. Bao, C. Zh, D. Z. Xue, J. H. Gao and X. B. Ren, *J. Phys. D: Appl. Phys.*, 2010, **43**, 465401.
5 G. Q. Kang, K. Yao and J. Wang, *J. Am. Ceram. Soc.*, 2011, 1–6.
6 A. Piorra, A. Petraru, H. Kohlstedt, M. Wuttig and E. Quandt, *J. Appl. Phys.*, 2011, **109**, 104101-1.
7 N. Ledermann, P. Muralt, J. Baborowski, S. Gentil, K. Mukati, M. Cantoni, A. Seifert and N. Setter, *Sens. Actuators, A*, 2003, **105**, 162–170.
8 W. F. Liu and X. B. Ren, *Phys. Rev. Lett.*, 2009, **103**, 257602-2.
9 B. C. Luo, D. Y. Wang, M. M. Duan and S. Li, *Appl. Phys. Lett.*, 2013, **103**, 122903.
10 V. V. Shvartsman, A. L. Kholkin, M. Tyunina and J. Levoska, *Appl. Phys. Lett.*, 2005, **86**, 222907.
11 N. A. Pertsev, A. Petraru, H. Kohlstedt, R. Waser, I. K. Bdikin, D. Kiselev and A. L. Kholkin, *Nanotechnology*, 2008, **19**, 375703.
12 V. V. Shvartsman and A. L. Kholkin, *Phys. Rev. B: Condens. Matter Mater. Phys.*, 2004, **69**, 014102.
13 W. Li, J. G. Hao, W. F. Bai and J. W. Zhai, *J. Sol-Gel Sci. Technol.*, 2013, **66**, 220–224.
14 B. C. Luo, D. Y. Wang, M. M. Duan and S. Li, *Appl. Surf. Sci.*, 2013, **270**, 377–381.
15 H. Uršič, J. Ricote, H. Amorín, J. Holc, M. Kosec and M. Algueró, *J. Phys. D: Appl. Phys.*, 2012, **45**, 265402.
16 X. Zhao, J. Y. Dai, J. Wang, H. L. W. Chan and C. L. Choy, *Phys. Rev. B: Condens. Matter Mater. Phys.*, 2005, **72**, 064114.
17 V. V. Shvartsman and A. L. Kholkin, *Appl. Phys. Lett.*, 2005, **86**, 202907.
18 V. V. Shvartsman and A. L. Kholkin, *Appl. Phys. Lett.*, 2007, **101**, 064108.
19 P. Sharma, T. Reece, D. W. Wu, V. M. Fridkin, S. Ducharme and A. Gruverman, *J. Phys.: Condens. Matter*, 2009, **21**, 485902.
20 V. V. Shvartsman, B. Dkhil and A. L. Kholkin, *Annu. Rev. Mater. Res.*, 2013, **43**, 423–449.
21 H. X. Fu and R. E. Cohen, *Nature*, 2000, **403**, 281.
22 H. Basantakumar Sharma, *Ferroelectrics*, 2013, **453**, 113–121.

www.spm.com.cn